Molecular Crystals and Liquid Crystals
Publication details, including instructions for authors and subscription information:
http://www.tandfonline.com/loi/gmcl16

Acoustical Streaming in a Film of Nematic Liquid Crystal

S. Candau [a], A. Ferre [a], A. Peters [a], G. Waton [a] & P. Pieranski [b c]

[a] Laboratoire d'Acoustique Moléculaire, Universitè Louis Pasteur, 4, rue Blaise Pascal, 67070, Strasbourg Cedex, France

[b] Laboratorie de Physique des Solides, Université de Paris-Sud, 91405, ORSAY Cedex, France

[c] Department of Physics, Brandeis University, Waltham, M.A., 02154, U.S.A.

Version of record first published: 20 Apr 2011.

To cite this article: S. Candau , A. Ferre , A. Peters , G. Waton & P. Pieranski (1980): Acoustical Streaming in a Film of Nematic Liquid Crystal, Molecular Crystals and Liquid Crystals, 61:1-2, 7-30

To link to this article: http://dx.doi.org/10.1080/00268948008081981

Mol. Cryst. Liq. Cryst., 1980, Vol. 61, pp. 7–30
0026-8941/80/6102-0007$04.50/0

Acoustical Streaming in a Film of Nematic Liquid Crystal

S. CANDAU, A. FERRE, A. PETERS, and G. WATON
Laboratoire d'Acoustique Moléculaire, Université Louis Pasteur, 4, rue Blaise Pascal 67070 Strasbourg, Cedex, France.

and

P. PIERANSKI†
Laboratoire de Physique des Solides, Université de Paris-Sud, 91405 ORSAY Cedex, France.

(*Received February 4, 1980*)

The streaming patterns induced in an homeotropically aligned nematic liquid crystal layer by an acoustic beam at oblique incidence have been investigated. The experimental observations are in good agreement with a two-dimensional streaming model.

INTRODUCTION

The investigation of acousto-optical effects in liquid crystals have been mainly motivated by the potential applications in the area of acoustic imaging. Most of the studies have been devoted to the birefringence effect induced by acoustic irradiation within a thin nematic liquid crystal layer placed between crossed polarizers. Several mechanisms, which are listed below, have been proposed to explain the observed phenomenon:

Instability due to second-order stresses.[1]

Static deformation resulting from a torque associated with the anisotropy of acoustic attenuation.[2,3]

Streaming due to gradients of acoustic radiation pressure.[4–8]

† Present address: Department of Physics, Brandeis University, Waltham, M.A. 02154, U.S.A.

All the experiments performed up to now have demonstrated that there is no characteristic threshold for the appearance of the acousto-optical effect, which excludes the instability mechanism.

In fact, there is considerable experimental evidence of acoustic streaming.[4–8] However, the streaming patterns, which have been shown to depend on both experimental geometry and acoustic excitation are not yet well established.

The optimal acousto-optical conversion seems to be obtained for a thin homeotropic layer sandwiched between two glass plates and irradiated under oblique incidence of acoustic waves. In that case, several mechanisms have been shown to coexist, which lead to complex streaming patterns.

In this work we have investigated the acousto-optical conversion using several liquid crystal cells of different configurations. These experiments allowed us to characterize the dominant streaming mechanism. We have compared the experimental results to the theoretical predictions from a two-dimensional streaming model.

I THEORETICAL

a) General equations for the acoustical streaming

The flow properties of fluids can be described from the following hydrodynamic equations.

Navier–Stokes equation

$$\rho\left(\frac{\partial \mathbf{u}}{\partial t} + (\mathbf{u}\cdot\nabla)\mathbf{u}\right) = -\nabla p + (\xi + \tfrac{4}{3}\eta)\nabla\nabla\cdot\mathbf{u} - \eta\nabla\times\nabla\times\mathbf{u} \tag{1}$$

Continuity equation

$$\frac{\partial \rho}{\partial t}\nabla + (\rho\mathbf{u}) = 0, \tag{2}$$

where ρ is the density, $\mathbf{u}$ the particle velocity, p the hydrostatic pressure, ξ the bulk viscosity and η the shear viscosity.

In the above equation, the variables can be expressed in series of ascending orders:

$$\begin{aligned} \rho &= \rho_0 + \rho_1 + \rho_2 + \cdots \\ p &= p_0 + p_1 + p_2 + \cdots \\ \mathbf{u} &= \mathbf{u}_1 + \mathbf{u}_2 + \cdots \end{aligned} \tag{3}$$

To derive the acoustic streaming equation, we have to consider the second order Navier–Stokes equation:[9]

$$-\nabla p_2 + (\xi + \tfrac{4}{3}\eta)\nabla\nabla \cdot \mathbf{u}_2 - \eta\nabla \times \nabla \times \mathbf{u}_2 = \mathbf{F} \tag{4}$$

with

$$\mathbf{F} = \rho_0 \langle |(\mathbf{u}_1 \cdot \nabla)\mathbf{u}_1^* + \mathbf{u}_1(\nabla \cdot \mathbf{u}_1^*) + \text{c.c.}| \rangle \tag{5}$$

where $\langle \cdots \rangle$ stands for time average.

Combining Eqs. (2), (4) (5) yields:

$$\eta\nabla^2\mathbf{u}_2 = \nabla p_2 - \mathbf{F} \tag{6}$$

where the acoustic force $\mathbf{F} = \mathbf{F}(\mathbf{r})$ depends on the experimental geometry.

In our experiments we are interested in the streaming induced by sound waves in a thin layer of oriented nematic liquid crystal, sandwiched between two solid substrates. Rigorously speaking, the Eq. (6) is not valid for anisotropic fluids and one should include in the equation of motion the anisotropic viscosity and the coupling between flow and director orientation.[10,11] However, since we are mainly interested in the streaming patterns, we can in a first approximation solve the equation of motion for a thin layer of isotropic fluid and consider separately the coupling between the director orientation and the dc flow. The solution of the acoustic equation of motion will depend on the experimental geometry as illustrated below.

1) *Normal incidence of the acoustic beam onto the cell.* Geometrical relations are presented in Figure 1a. The acoustic streaming force is given as:[9]

$$\begin{aligned} \mathbf{F} &= (0, 0, F) \qquad |x| < a' \\ &= 0, \qquad a' < |x| < b' \\ F &= \rho_0 \alpha I \end{aligned} \tag{7}$$

where α is the absorption constant and I the acoustic intensity.

This case has been treated theoretically by Nagaï *et al.*[7] and leads to the velocity and orientation patterns schematically represented in Figure 1a. In the central part of the cell, the flow is directed along the axis $0z$ perpendicular to the plates. The maximum tilt of the molecules of liquid crystal with respect to their initial orientation occurs at the edge of the acoustic field.

2) *Oblique incidence of the acoustic beam onto the cell.* Let us consider an acoustic beam falling on the liquid crystal cell with an incidence angle θ in the plane $x0z$ (cf. Figure 1b). The acoustic streaming force within the

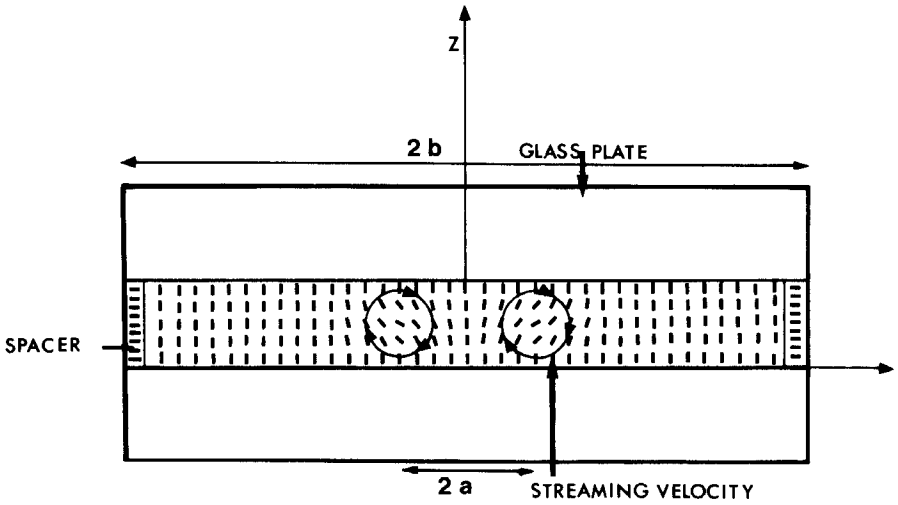

(a)

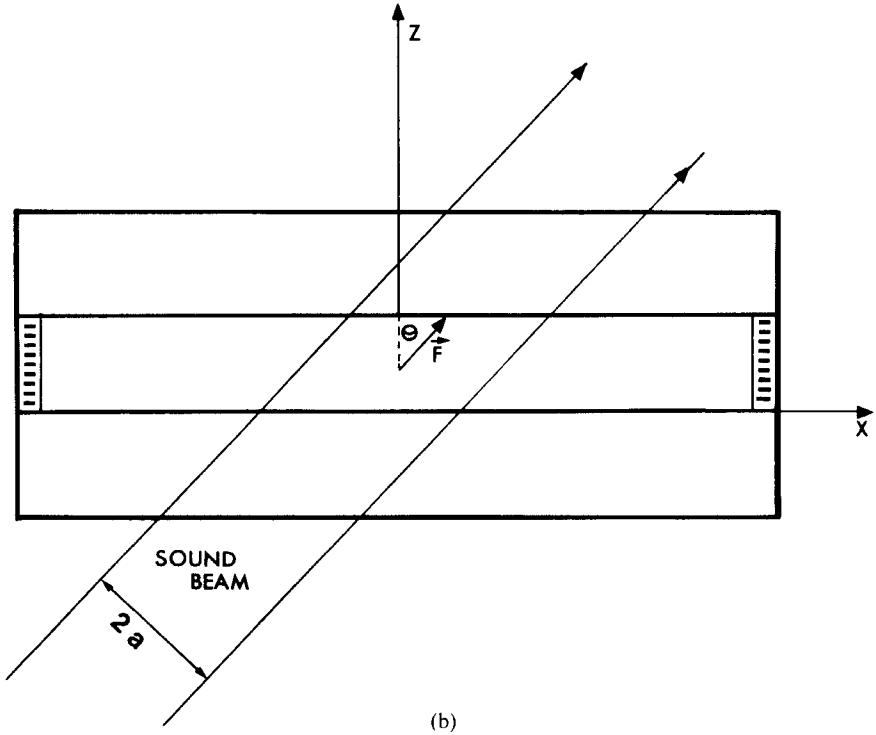

(b)

FIGURE 1 Experimental configurations for normal (a) and oblique (b) incidences of the acoustic beam. Small bars express liquid crystal molecules. One takes the z-axis as the direction of the initial orientation, and the x-axis is chosen so that x-z plane contains the tilt nematic axis. 2a and 2b are the widths of the ultrasonic beam and the cell, respectively.

irradiated volume V is given as:

$$\mathbf{F} = (F \cos\theta, 0, F \sin\theta) \tag{8}$$

Outside V

$$\mathbf{F} = 0.$$

The streaming pattern inside and in the vicinity of the sound irradiated volume is rather complicated for the following reasons:

i) The acoustic force has components in both z and x directions, which produce a three-dimensional streaming.

ii) The distribution of the acoustic intensity is not constant across a section of the beam but is rather characterized by a Gaussian profile.

iii) Some longitudinal acoustic energy is converted in the layered system into surface like and guided modes which interact and produce a local periodic streaming.[4, 5, 8]

The problem is somewhat simpler if one investigates the part of the liquid crystal layer located far away from the cross section of the beam. In this region of space, one expects to observe a two-dimensional streaming resulting only from the F_x component of the acoustic force. Therefore the hydrodynamic problem will consist to find the velocity pattern $\mathbf{u}_2(x, y, z)$ when a quasi uniform streaming with a velocity u_{0x} is induced in a small volume V around the origin.

Outside the volume V the Eq. (6) can be written:

$$\eta \Delta \mathbf{u}_2(x, y, z) = \nabla p_2 \tag{9}$$

One looks for solutions of the following form:

$$\mathbf{u}_2(x, y, z) = \mathbf{u}_2(x, y) \cdot f(z) \tag{10}$$

The condition of no slipping at the planes $z = \pm d/2$ is satisfied if we write:

$$\mathbf{u}_2(x, y, z) = \mathbf{u}_2(x, y) \cdot \left(1 - \frac{z^2}{(d/2)^2}\right) \tag{11}$$

At distances far longer than the radius of the cross section of the ultrasound beam, one can neglect the rates of variation of u_{2x}, u_{2y} with respect to x, y in comparison with their rates of variation with respect to z. Then the solution of Eq. (9) is given by:

$$\mathbf{u}_2(x, y) = -\frac{d^2}{8\eta} \nabla p_2 \tag{12}$$

The Eq. (12) and the continuity equation, $\nabla \cdot \mathbf{u}_2 = 0$ yield:

$$\Delta p_2 = 0 \tag{13}$$

There is a close analogy between the streaming problem considered here and the problem of a two-dimensional electric dipole. In the latter case the electric field **E** and the potential Φ are given by the following relations:

$$\mathbf{E} = -\nabla\Phi \quad \text{and} \quad \Delta\Phi = 0 \tag{14}$$

which are equivalent to Eqs. (12) and (13).

The solutions of (14) for a two-dimensional dipole can be expressed in cylindrical coordinates (r, ϕ) as:[12]

$$\Phi \sim p_2 = \text{const} \frac{\cos\phi}{r} \tag{15}$$

$$E_x \sim u_{2x} = \text{const} \frac{\cos 2\phi}{r^2}$$

$$E_y \sim u_{2y} = \text{const} \frac{\sin 2\phi}{r^2} \tag{16}$$

The stream lines obtained from Eqs. (16) are circles tangent to $0x$ with their centers on $0y$. (Cf. Figure 2).

We have also reported on Figure 2 the lines of equal modulus of the velocity, which are circles centered on the origin according to the equation:

$$|\mathbf{u}_2| = \frac{\text{const}}{r^2} \tag{17}$$

The constant factor in front of Eq. 17 will depend on the acoustic characteristics.

Inside the sound irradiated volume

$$\nabla p_2 \sim \alpha I$$

Then by continuity one must have:

$$|\mathbf{u}_2| \sim \alpha I \tag{18}$$

Equation (12), (17), and (18) show that

$$|\mathbf{u}_2| \sim \frac{\alpha I d^2}{\eta} \frac{1}{r^2} \tag{19}$$

b) Flow reorientation of the nematic molecules

Let us consider an homeotropically aligned layer of nematic liquid crystal. The stationary streaming induces a shear-flow reorientation of the nematic molecules. We want to calculate the z dependence of the tilt angle of the director from the z axis, given x and y. For small θ, the equation of the

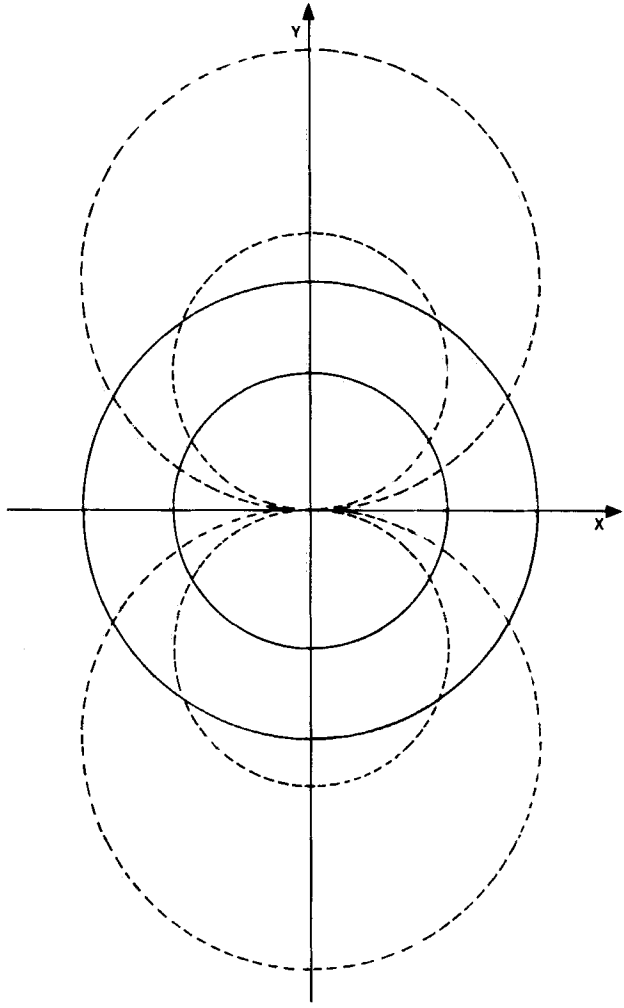

FIGURE 2 Two-dimensional streaming pattern induced by an acoustical force directed along the x-axis. The dashed circles represent the stream lines. The full circles represent the lines of equal velocity.

balance of torques is[10,11]:

$$K_{33}\frac{\partial^2\theta}{\partial z^2} + \alpha_2\frac{\partial u_2}{\partial z} = 0 \tag{20}$$

where

$$u_2 = |\mathbf{u}_2(x, y)|\, f(z) \tag{21}$$

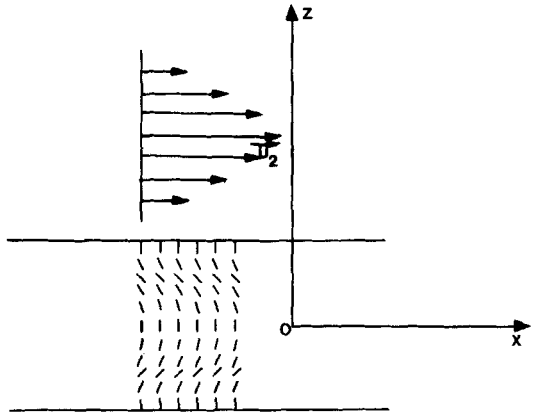

FIGURE 3 Orientation pattern of an homeotropic liquid crystal layer, induced by a stationary flow along x.

K_{33} is Frank's bend elastic constant[13] and α_2 is Leslie's shear-torque coefficient.[10]

Assuming a Poiseuille distribution for $f(z)$ (cf. Eq. 11) and using the boundary conditions $\theta = 0$ for $z = \pm d/2$, one obtains by integration of Eq. 20

$$\theta = \frac{\alpha_2 u_{20}}{3K_{33}} z\left[\frac{z^2}{(d/2)^2} - 1\right] \tag{22}$$

where u_{20} represents $u_2(z = 0)$. In Figure 3 we have schematically represented the reorientation pattern for a flow directed along the x axis. One observes that the variation of the induced tilt is symmetrical with respect to the x axis.

c) Optical patterns exhibited by a cell placed between crossed polarizers

If the nematic film is placed between crossed polarizers with their axis along $0x$ and $0y$, the optical transmission of the cell is given by:[14]

$$\frac{J}{J_0} = \sin^2(2\beta)\sin^2(\delta/2) \tag{23}$$

where J and J_0 are, respectively, the transmitted and incident light intensities, β is the angle between the polarization of the incident beam and the projection of the optic axis of the material, δ is the phase difference between the

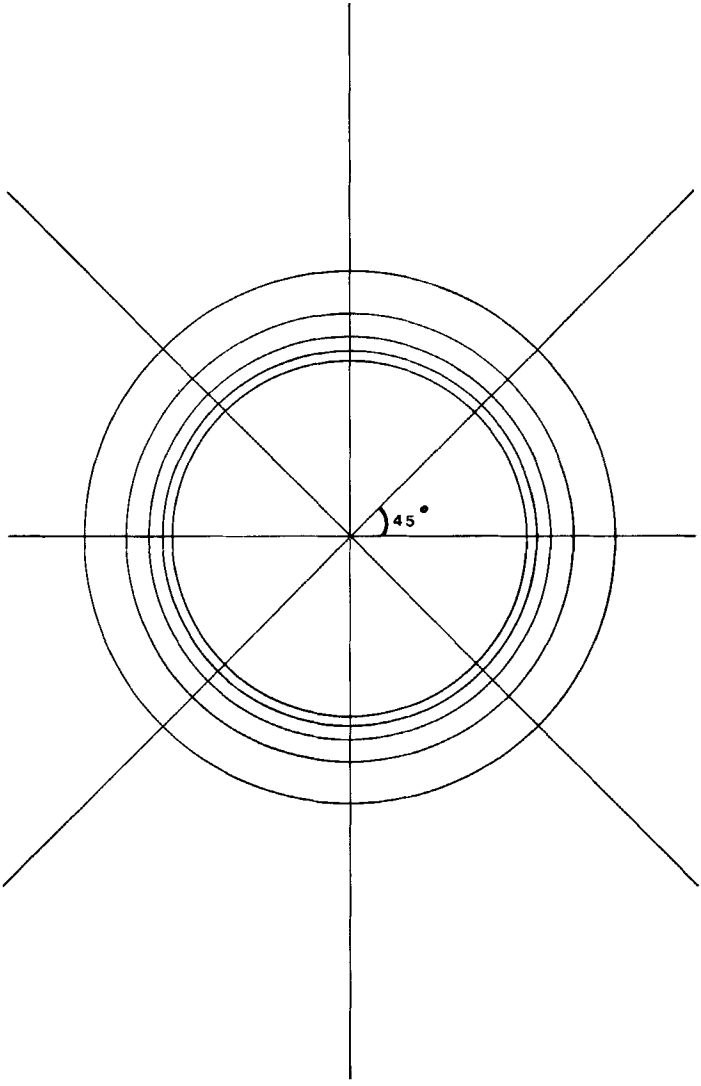

FIGURE 4 Theoretical optical pattern for an homeotropic liquid crystal layer between crossed polarizers oriented along x and y axes. The straight lines and the circles represent the isoclines and the isochromes respectively.

ordinary ray and the extraordinary ray:

$$\delta(x, y, z) = \frac{2\pi}{\lambda}(n_e - n_0)\int_{-d/2}^{d/2} \theta^2(x, y, z)\mathrm{d}z \tag{24}$$

where λ is the optical wavelength, and n_e and n_0 are the refractive indices of the extraordinary ray and ordinary ray respectively.

Since $\theta(x, y, z)$ is proportional to u_{20} (cf. Eq. 22) the lines of constant phase shift δ correspond to lines of equal velocity, which according to Eq. 17 are circles centered on the origin. Therefore the optical pattern will exhibit dark rings corresponding to $\delta = 2K\pi(K = 1, 2, \ldots)$, as illustrated in Figure 4.

The spacing between the rings can be obtained from Eqs. (17), (19), (23) and obeys the condition

$$KR_K^4 = \text{const}(K = 1, 2, \ldots) \tag{25}$$

where R_K represents the radius of the ring of order K.

The optical patterns exhibit also dark lines corresponding to tilt angles in the planes of the polarizers. The isocline lines can be obtained from the stream lines represented in Figure 2. For crossed polarizers along $0x$ and $0y$, one should observe dark straight lines crossing at the center at 45° angle as shown in Figure 4.

Finally, the dependence of the transmitted light intensity on the acoustical and geometrical parameters and on the liquid crystal characteristics is obtained from Eqs. (19), (22) and (23).

$$\frac{J}{J_0} \sim \frac{\alpha^4 I^4 d^{14}}{\eta^4} \tag{26}$$

II EXPERIMENTAL TECHNIQUE

The experimental set-up is shown in Figure 5. The liquid crystal cell is immersed in a temperature regulated water bath. The light beam is polarized, passes at normal incidence through the cell, is analyzed and is then either focused on a photodiode or projected on a screen. Circular polarization of the light can be obtained by placing quarter wavelength plates in front of the polarizer and the analyzer; this eliminates the dark isoclines in the optical pattern. The ceramic transducers operating at 2.8 MHz, 4.7 MHz, 8.4 MHz are mounted vertically and the acoustic beam falls at adjustable incidence on the cell. An acoustical lens of focal length 4.2 cm is used for experiments requiring a focusing of the acoustic beam. The voltage applied to the transducer is calibrated using a torsion pendulum as described earlier[17] to give the acoustic intensity in the water at the position of the

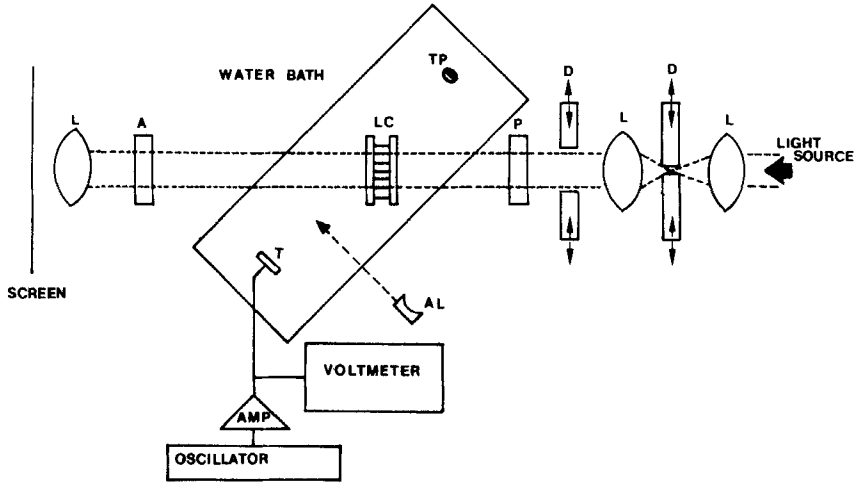

FIGURE 5 Experimental set-up; *T*: transducer. *AL*: acoustical lens. *LC*: liquid crystal cell. *TP*: torsional pendulum. *D*: diaphragm. *L*: lens. *P*: polarizer. *A*: analyser.

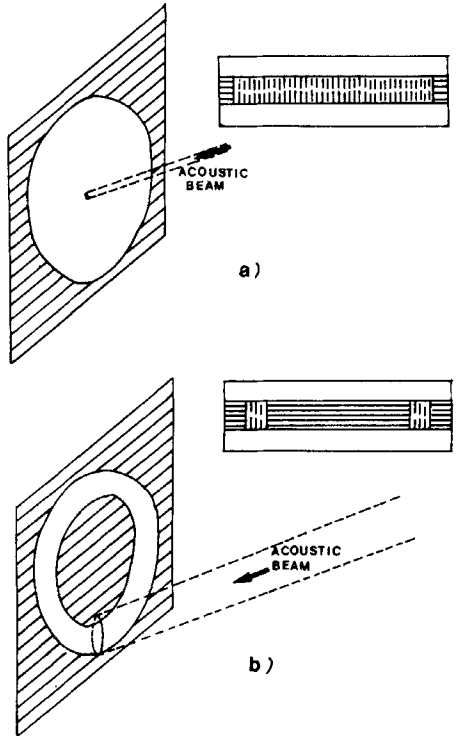

FIGURE 6 Test cells: a) annular, b) circular.

liquid crystal cell. The exact acoustic intensity in the liquid crystal is not known, but for a constant frequency and angle of incidence, it is proportional to the calibrated intensity in the water at the position of the crystal cell. Furthermore, the torsional pendulum device allows us to measure the acoustic intensity transmitted through the cell.

The liquid crystal sample was 4'-*n*-pentyl-4-cyanobiphenyl (5CB) purchased from BDH Chemicals, Ltd., and used without further purification. The acousto-optical conversion cell consisted of a layer of 5CB with a thickness varying from 150 to 550 μm sandwiched between two thin transparent glass plates (150 μm thick) separated by a Mylar spacer. Homeotropic alignment (molecules normal to the glass surfaces) was achieved by applying a thin layer of lecithin on the two inner surfaces of the glass plates. Two different cell configurations have been used as shown in Figure 6. In the cells represented on Figure 6a the area occupied by the liquid crystal was about $40 \times 40\ mm^2$. The acoustic beam was focused on the center of the cell, the area of the focus being around $0.1\ cm^2$. The annular cells (cf. Figure 6b) were irradiated with a sound beam of diameter equal to the width of the channel (5 mm).

III EXPERIMENTAL RESULTS

a) Annular cells

The major aim of the experiments performed on annular cells was to investigate the streaming mechanism far away from the acoustic perturbation.

Earlier studies were carried out in the sound irradiated region. As mentioned before, several mechanisms coexist in this region. More especially, for some geometrical configurations, the transmitted optical signal is modulated by striations associated with the interaction of surface like and guided modes.[8,15,16] The earlier experiments also demonstrated that for a particular cell thickness and a particular ultrasonic frequency, only a rather narrow range of angles of incidence of the ultrasonic beam provides a strong optical signal. This angular dependence of the sensitivity has been shown to be mainly related to the cell structure and it is important to determine whether the optimal sensitivity does correspond to a maximum of acoustic intensity within the cell as expected from the two-dimensional streaming model.

In the annular cells, the effect observed on a zone diametrically opposite to the irradiation area, can result only from the streaming process described in the theoretical section.

The photographs of Figure 7 illustrate the effect of the acoustic irradiation on the orientation of the liquid crystal. The acoustic beam was directed on

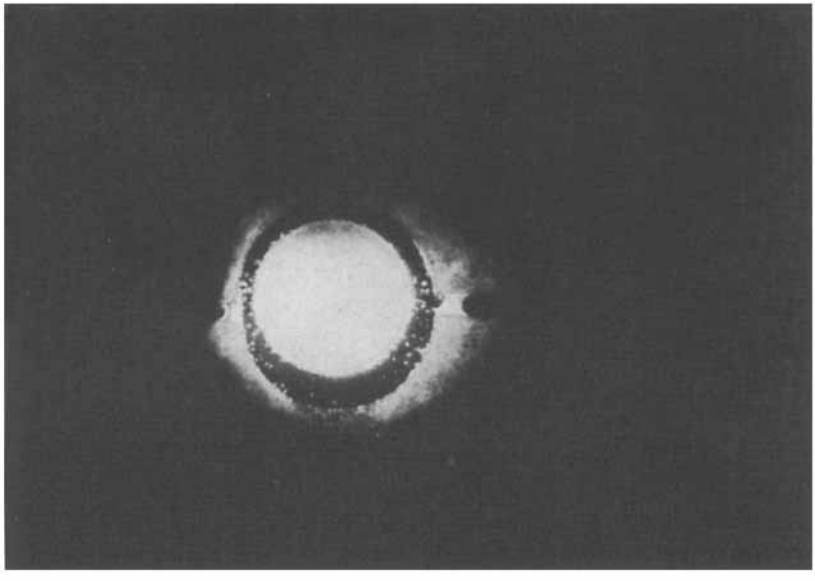

(a)

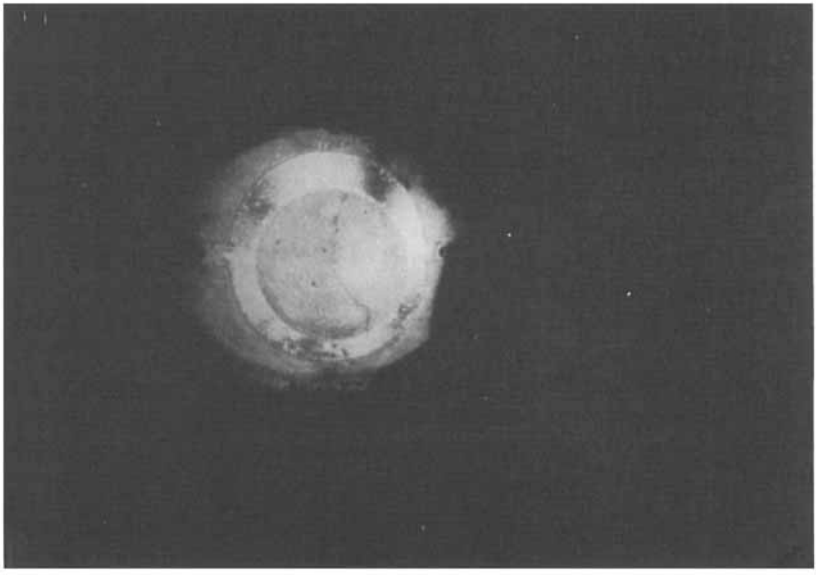

(b)

FIGURE 7 Annular liquid crystal cell between crossed polarizers. a) Without acoustic irradiation. b) Under acoustic irradiation of the lower part of the chennel $d = 200\ \mu m$, $f = 2.82$ MHz, $I = 10$ mw/cm^2.

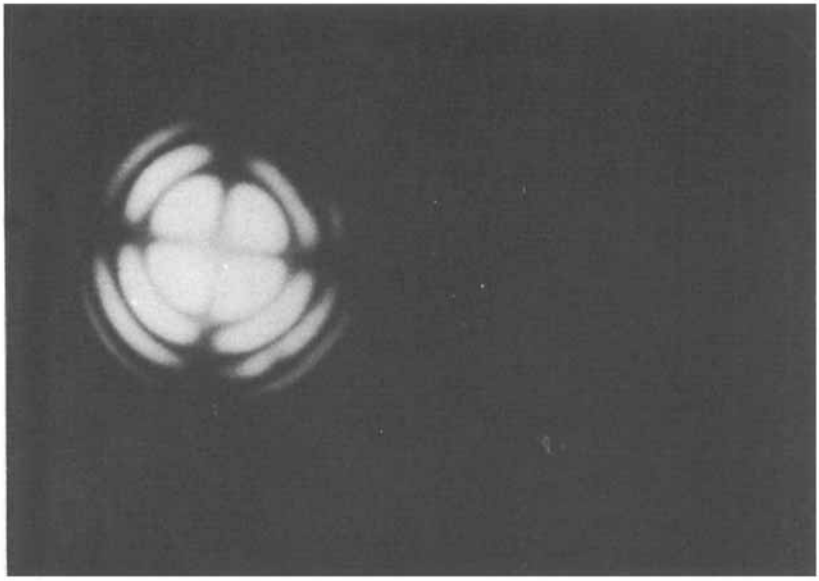

(a)

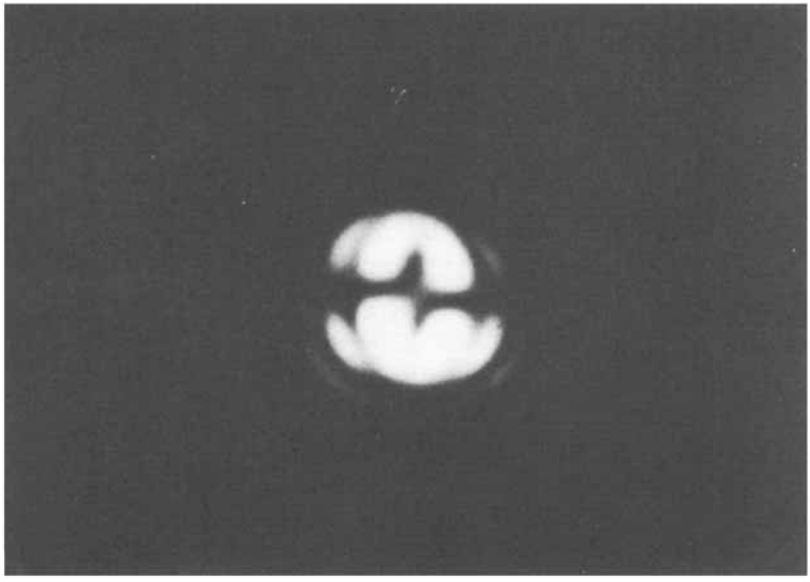

(b)

FIGURE 8 Conoscopic observations of the upper part of the liquid crystal channel. a) Without acoustic irradiations. b) Under acoustic irradiation of the lower part of the channel: the polarizers are oriented along directions tangent and normal to the axis of the channel $d = 200$ μm, $f = 2.82$ MHz, $I = 10$ mw/cm^2.

the lower part of the channel. In order to prevent any stray irradiation of the upper part of the channel, only the lower half of the cell was immersed.

Under acoustic irradiation the whole channel becomes bright. On the other hand, if the acoustic beam is directed onto the spacer, out of the liquid crystal, there is no visible effect. This observation confirms then the existence of a long distance transverse streaming on the liquid crystal.

Further indication on the reorientation process is given by conoscopic investigation. In the absence of sound irradiation, the conoscopic pattern obtained for an homeotropic texture is a Maltese cross (cf. Figure 8a).

A reorientation of the liquid crystal director with the symmetry shown in Fugure 3 should produce a deformation of the optical pattern with no shift of its center. That is what is observed experimentally on the photograph (8b) obtained in the upper part of the channel.

We have next investigated the sensitivity of the liquid crystal cell as a function of the incidence angle of the acoustic beam on the cell. The angular dependence of the transmitted optical intensity between crossed polarizers at constant acoustic intensity (10 mw/cm^2) exhibits a sharp peak around

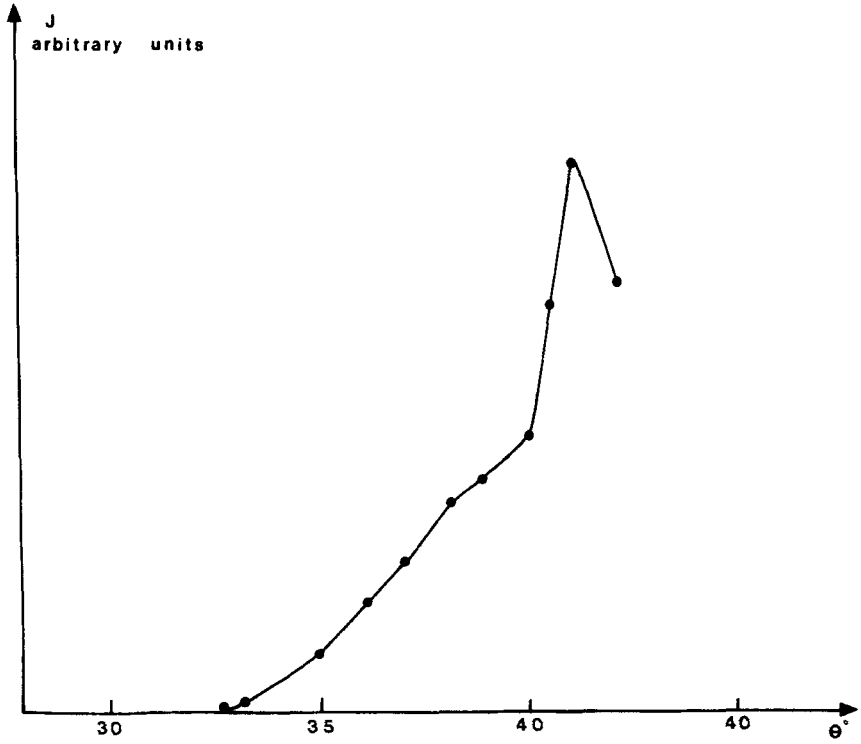

FIGURE 9 Angular dependence of the sensitivity of the cell. $d = 200\ \mu m$, $f = 2.82$ MHz, $I = 10$ mw/cm^2.

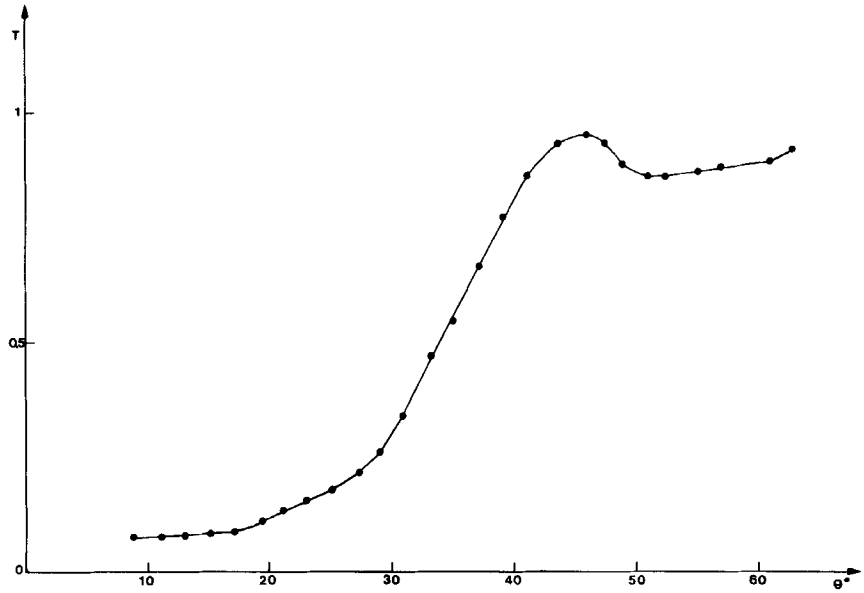

FIGURE 10 Angular dependence of the acoustical transmission coefficient $d = 200\ \mu m$, $f = 2.82$ MHz, $I = 10$ mw/cm^2.

$\theta = 41°$ (cf. Figure 9). Indeed Figure 10 shows that this peak corresponds to a maximum of the acoustic transmission $T = I/I_0$ of the cell as expected from the theoretical model.

In Figure 11 we have reported a Log-Log plot of the optical transmission coefficient $\tau = (J - J_0/J_0)$ versus U^2 which is proportional to I(U voltage across the transducer). In the intensity range corresponding to a phase difference δ varying from 0 to π (cf. Eq. (23)), one obtains a straight line with a slope of 3.3. This slope is lower than the theoretically predicted value which is 4. It is also slightly lower than the value obtained when the measurement is performed within the sound irradiated region. In this regard, one should remark that rather high acoustical intensity is required to induce flow in the upper part of the annular channel. Some visible disinclinations are created, which can slow down the flow and lead to a smaller exponent for the $\tau(I)$ variation.

b) Circular cells irradiated at their center by a focused ultrasonic beam

The experimental geometry is shown schematically in Figure 6a. If the acoustical intensity is sufficiently large, the flow pattern can be directly visualized from the motion of the dislinations as shown in the photograph (12a).

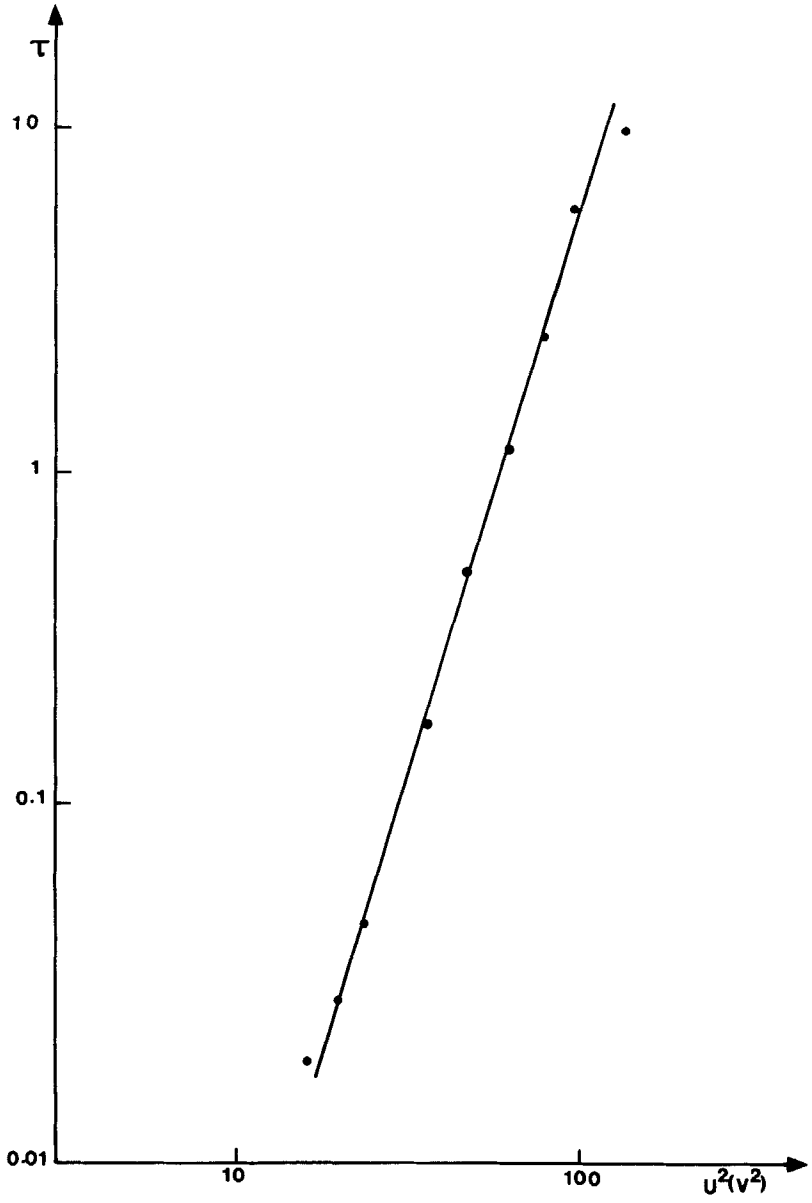

FIGURE 11 Log-Log plot of the optical transmission τ versus U^2 $d = 200$ μm, $\theta = 38°$ $f = 2.82$ MHz.

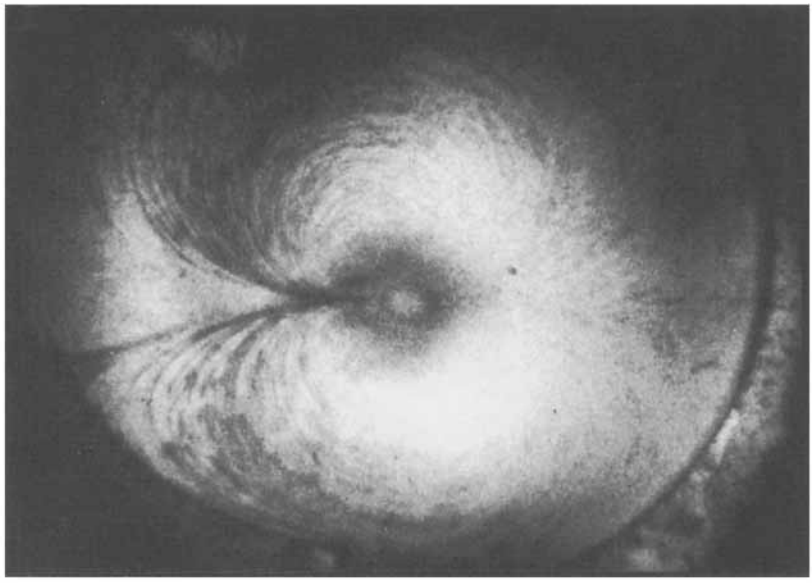

(a)

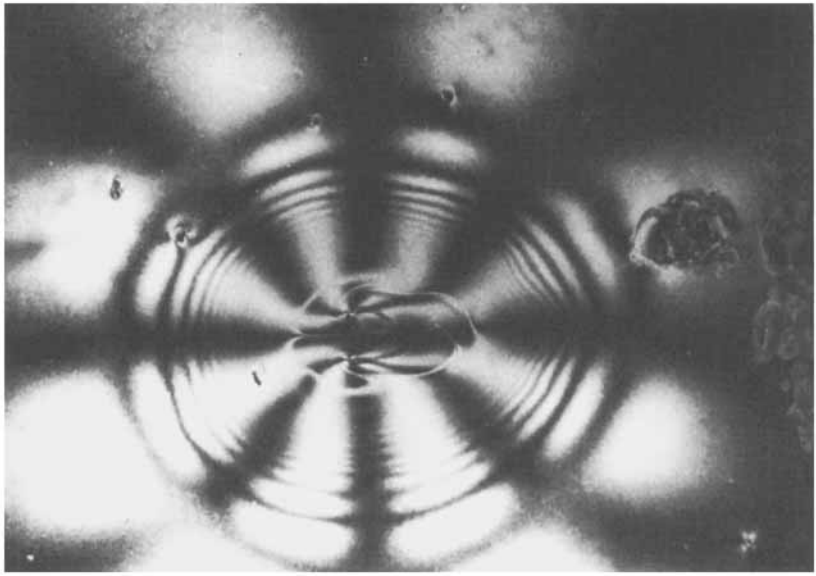

(b)

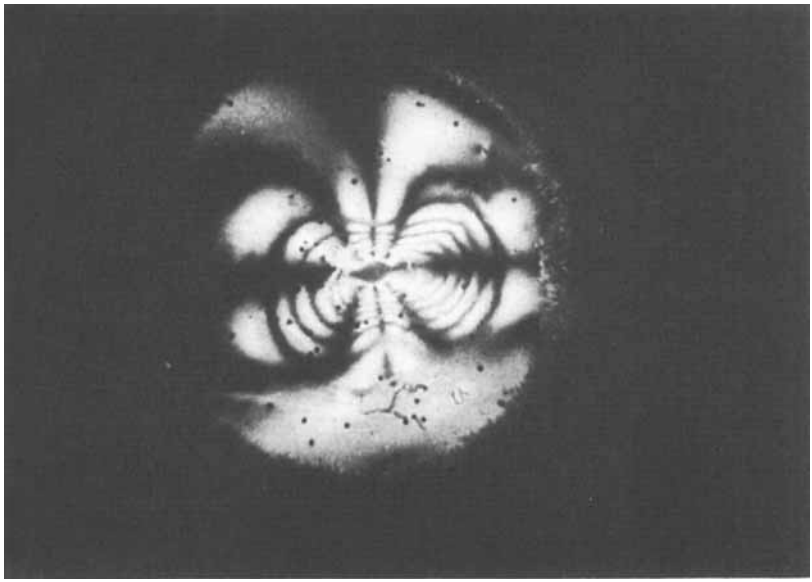

FIGURE 12 Photographs illustrating the two-dimensional streaming effect. The acoustic force is directed from the left to the right. a) With unpolarized light and high acoustical intensity ($I \sim 40$ mw/cm^2) the streaming is evidenced by the motion of disclinations. One clearly sees the focus of the ultrasonic beam in the center of the cell $d = 200$ μm, $f = 2.82$ MHz. b) and c) Between crossed polarizers. b) $d = 550$ μm, $f = 4.4$ MHz. c) $d = 200$ μm, $f = 2.82$ MHz.

In this photograph, one observes clearly quasi-circular stream lines tangent to the focal spot in which they are generated. The flow is directed along the projection of the acoustic force in the plane of the cell (from the left to the right, in the present case). This streaming profile is in qualitative agreement with the theoretical pattern described in Figure 2. The optical pattern obtained when the liquid crystal cell is viewed between crossed polarizers is also rather close to the pattern predicted from the two dimensional streaming model as revealed by the comparison between Figure 4 and photograph (12b). More especially, one observes isoclines crossing at 45° angle and isochromatic lines, approximately circular and centered on the sound irradiated spot. One must however remark that the isochromatic lines are somehow elongated along the direction of the acoustic force. This dissymetry which increases with the angular incidence of the acoustic beam may be attributed to the presence of reflected acoustic waves within the liquid crystal layer which propagate away from the irradiated spot and provide a supplementary contribution to the flow. Another feature of the pattern is the presence of some disclinations within the sound irradiated volume. These disclinations which appear at rather small acoustical intensities do

not seem to disturb the long distance streaming, at least for large thicknesses of the liquid crystal layer and high frequencies. In fact, the distortion of the optical pattern increases when the ratio d/λ_s (d, thickness of the liquid crystal layer, λ_s acoustic wavelength) decreases. For $d < \lambda_s/2$ the streaming pattern becomes very complex and cannot be interpreted within the framework of the present model (see photograph 12c). This was first observed and studied in detail by Perbet and Hareng.[19] On the other hand for $d > \lambda_s/2$ the experimental patterns can be analyzed in order to attempt a quantitative fit to the two-dimensional streaming model.

We have first investigated the interspacing of the isochromatic lines. In Figure 13 we have reported a log-log plot of the radii R_K of the isochromatic circles as a function of the order K. The radii have been measured in the half plane located backward with respect to the direction of the acoustic force (the left half of the photograph 11b), where the shape of the isochromatic lines is rather well described by half-circles. The data fit a straight line as

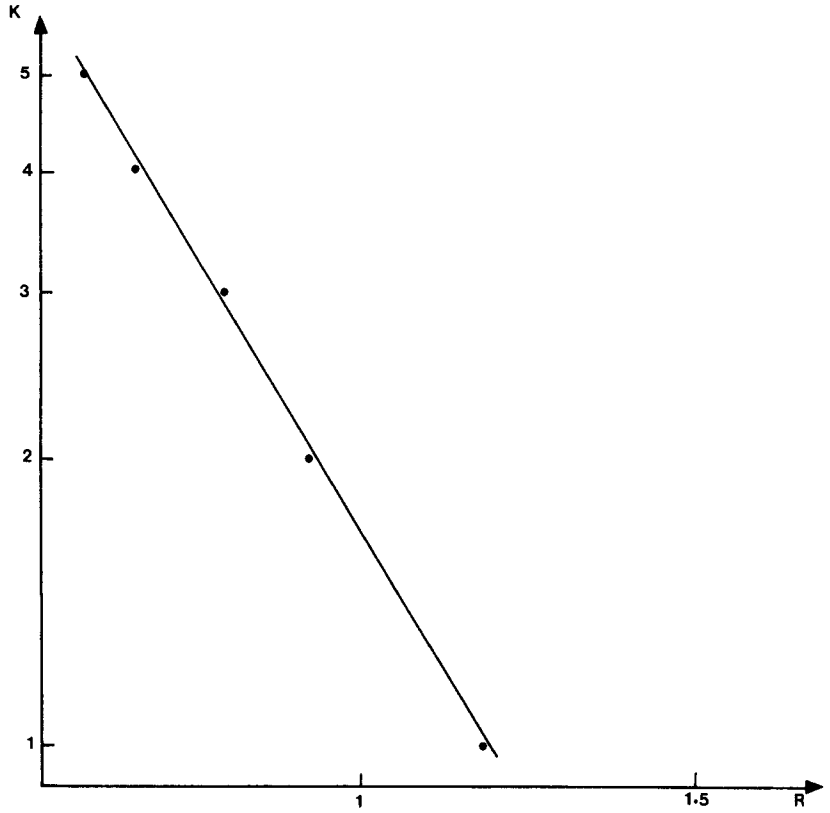

FIGURE 13 Log-Log plot of the radius R_K of the isochromes versus the order K.

shown in Figure 12. The slopes, which range from -3.2 to 3.9 depending on the angular incidence of the acoustic beam and the ratio d/λ_s, are rather close to the theoretical value (-4).

We have next investigated the dependence of the radius R_K of a given isochromatic circle on the acoustical intensity I.

By combining the condition $\delta = \text{const}$ with Eq. 19, one obtains the following relationship between R_K and I, keeping constant all the other parameters:

$$\frac{I}{R_K^2} = Ct \tag{27}$$

In Figure 14 we have plotted an example of the variation of $R_1(K = 1)$ with the voltage U across the acoustic transducer. One obtains a straight line as predicted from the above expression.

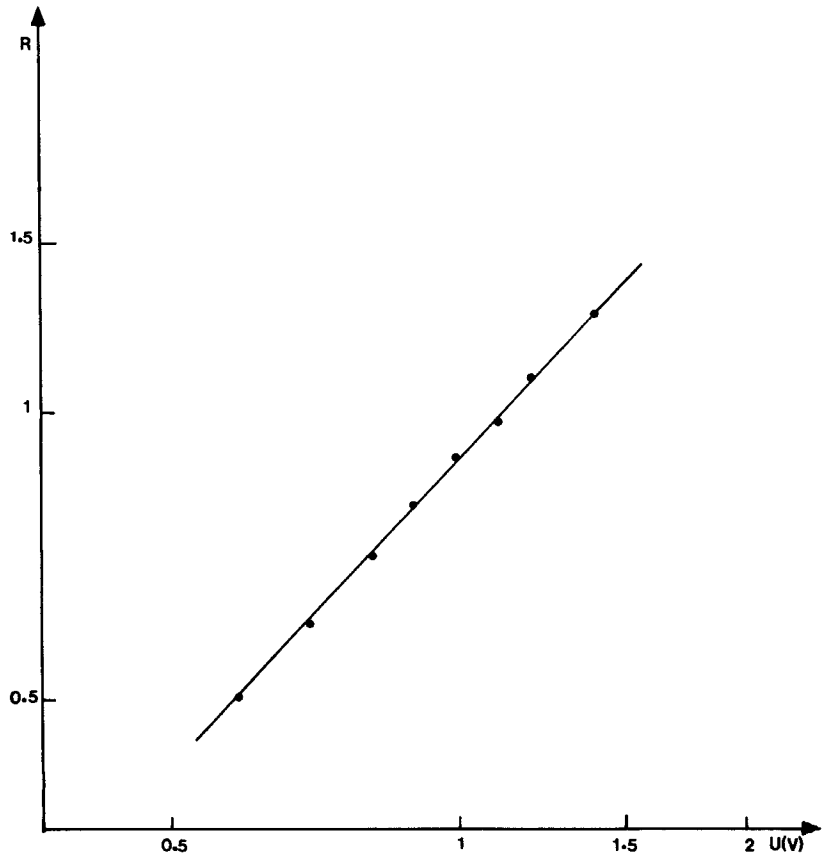

FIGURE 14 Variation of the radius of the first order isochrome with the voltage U across the transducer.

Finally, one can attempt to investigate the influence of the liquid crystal thickness on the sensitivity of the detector.

In principle, this can be done by looking at the dependence of the radius R_K of an isochromatic ring of a given order, with the thickness of the liquid crystal layer, at constant intensity. The condition δ = const. together with Eqs. (19), (22) and (24) yield:

$$\frac{I^2 d^7}{R_K^4} = \frac{U^4 d^7}{R_K^4} = Ct \tag{28}$$

However, the effect of the liquid crystal thickness is difficult to investigate for the following reasons:

i) For thicknesses smaller than $\lambda_s/2$, the streaming mechanisms become complex as mentioned before.

ii) The angular dependence of the effective acoustical intensity within the cell varies with the liquid crystal thickness. More especially the maximum of sensitivity, (monitored by the radius R_K of a given isochromatic line) is obtained at an angle which depends on the thickness. A meaningful comparison between cells of different thicknesses can be made if the measurements are performed at the angles of maximum sensitivity.

Using this procedure, we have measured the ratio U^4/R_1^4 for two cells of thickness 200 μm and 550 μm respectively and we have obtained the following results, in reasonable agreement with the prediction of Eq. (28).

$$d = 200\ \mu\text{m}\ \frac{U^4 d^7}{R_4^1} = 1.35\ 10^{-9}\ V^4\ \text{cm}^3$$

$$d = 550\ \mu\text{m}\ \frac{U^4 d^7}{R_1^4} = 1.52\ 10^{-9}\ V^4\ \text{cm}^3$$

CONCLUSION

We have shown that an acoustic beam falling at oblique incidence on a thin homeotropic liquid crystal layer induces a streaming in the plane of the cell, which extends far away from the irradiated zone.

The optical patterns observed when the cell is viewed between crossed polarizers can be quantitatively interpreted by a two-dimensional streaming model provided that the thickness of the liquid crystal layer is larger than half the acoustic wavelength. These results explain why it is not possible to obtain clear ultrasonic images with conventional liquid crystal cells. On

the other hand, the spatial resolution is considerably improved by dividing the nematic cell into a matrix of liquid crystal arrays separated by thin strip spacers which prevent acoustic streaming between arrays.[15–18].

Acknowledgments

It is a pleasure to thank E. Guyon, M. Hareng and J. N. Perbet for helpful comments and discussions during the course of this study. The authors are very grateful to M. Hareng and J. N. Perbet for having communicated their results prior to publication.

References

1. W. Helfrich, *Phys. Rev. Lett.*, **29**, 1583 (1972).
2. J. L. Dion, *C. R. Hebd. Séan. Acad. Sci.*, **B284**, 219 (1977).
3. J. L. Dion and A. D. Jacob, *Appl. Phys. Lett.*, **31**, 490 (1978).
4. K. Miyano and Y. R. Shen, *Appl. Phys. Lett.*, **16**, 281 (1976).
5. K. Miyano and Y. R. Shen, *Phys. Rev.*, **A15**, 2471 (1977).
6. C. Shripaipan, C. Hayes, and G. T. Fang, *Phys. Rev.*, **A15**, 1297 (1977).
7. S. Nagai, A. Peters and S. Candau, *Rev. Phys. Appl.*, **12**, 21 (1977).
8. S. Letcher, J. Lebrun and S. Candau, *J. Acoust. Soc. Am.*, **63**, 55 (1978).
9. See for instance: W. Nyborg, *Physical Acoustics*, vol. II B (Mason, W. P. ed., Academic Press, New York) 1968.
10. F. M. Leslie, *Quart. J. Mech. Appl. Math.*, **19**, 357 (1966).
11. See for instance: P. G. de Gennes, *The Physics of Liquid Crystals*, (Oxford, London, 1974).
12. See for instance: E. Durand, *Electrostatique et Magnétostatique*, (Masson et Cie, ed., Paris) 1953.
13. F. C. Frank, *Disc. Faraday Soc.*, **25**, 19 (1958).
14. See for instance: M. Born and E. Wolf, *Principles of optics* (Pergamon, London, 1970), chap. XIV.
15. J. Lebrun, S. Candau and S. V. Letcher, *J. Phys. C3*, **40**, 298 (1979).
16. J. N. Perbet, M. Hareng and S. Le Berre, *Rev. Phys. Appl.*, **14**, 569 (1979).
17. S. Nagai and K. Ilzuka, *Japan J. Appl. Phys.*, **17**, 723 (1978).
18. S. Nagai and K. Ilzuka, *Mol. Cryst. Liq. Cryst.*, **45**, 83 (1978).
19. J. N. Perbet and M. Hareng, Private Communication.